Harmonic generation in bent graphene with artificially enhanced spin-orbit coupling

Arttu Nieminen and Marco Ornigotti*
Physics Unit, Photonics Laboratory, Tampere University, FI-33720 Tampere, Finland

(Received 22 April 2022; accepted 12 October 2022; published 25 October 2022)

We theoretically investigate the nonlinear response of bent graphene in the presence of artificially enhanced spin-orbit coupling, which can occur either via adatom deposition or by placing the sheet of bent graphene in contact with a spin-orbit-active substrate. We discuss the interplay between the spin-orbit coupling and the artificial magnetic field generated by the bending for the cases of both Rashba and intrinsic spin-orbit coupling. For the latter, we introduce a spin-field interaction Hamiltonian addressing directly the electron spin as a degree of freedom. Our findings reveal that in this case, by controlling the amount of spin-orbit coupling, it is possible to significantly tune the spectrum of the nonlinear signal, achieving, in principle, efficient conversion of light from the terahertz to UV region.

DOI: 10.1103/PhysRevA.106.043517

I. INTRODUCTION

Since its discovery in 2004 [1], graphene has attracted a lot of interest in the scientific community, mainly due to its exquisite, and unexpected, electronic, mechanical, and thermal properties [2,3] but also due to it fascinating optical properties, such as universal absorption [4], ultrafast broadband response [5], and large nonlinear optical responses [6,7], to name a few. Most of these properties derive directly from the presence, in the band structure of graphene, of Dirac cones, i.e., points in k space, where valence and conduction bands touch, thus giving rise to a gapless linear dispersion [8]. Monolayers of graphene also admit spin-orbit coupling (SOC) in the form of both intrinsic (Δ_I) and Rashba (Δ_R) coupling, the former originating as a true SOC due to the relativistic nature of electrons in graphene, with the latter occurring only in the presence of an external electric field [8]. For the particular case of $\Delta_I > \Delta_R/2$, Kane and Mele discovered, for a finite monolayer of graphene, that the gap opened by SOC at the Dirac points sustains topologically protected edge states near its boundary [9], where spin-dependent impurity backscattering is strongly suppressed, resulting in the so-called quantum spin Hall (QSH) edge states. The discovery of Kane and Mele, moreover, was so influential that it gave birth to the exciting field of topological insulators [10], which, soon after its discovery in the context of condensed-matter physics, started affecting other fields of physics, giving rise to new ideas, such as topological photonics [11,12], topological mechanics [13], and topological atomic physics [14].

The QSH effect, however, is quite hard to observe experimentally in pristine graphene since the value of the intrinsic SOC is too small to allow its experimental verification [15–17]. The QSH state, however, has been experimentally observed in other systems, such as HgTe quantum wells [18], InAs/GaSb quantum wells [19], and WTe_2 [20], to name a few. To overcome the problem of small SOC in graphene, several different strategies have been proposed, ranging from increasing the Rashba coupling by depositing graphene on Ni surfaces [21,22] to a significant increase of the intrinsic SOC by adatom deposition of different compounds [23], such as indium, thallium, and Bi_2Te_3 nanoparticles, the latter representing the first experimental evidence of the occurrence of the QSH effect in graphene with artificially enhanced SOC [24].

Contextually, several works investigated the effect of Rashba [25–27] and intrinsic SOC on the electronic structure of graphene in the presence of magnetic fields [28]. The latter, in particular, has attracted considerable attention in recent years because it can be realized by applying strain or bending to single- and multilayer two-dimensional (2D) materials [29,30], resulting in high artificial magnetic fields, which, contrary to real ones, cannot break time-reversal symmetry. A comprehensive review of the topic can be found in Ref. [31].

Interestingly, however, only a few works have investigated the effects of (pseudo)magnetic fields in the nonlinear optical response of graphene, and they have mainly focused on estimating how the third-order nonlinear susceptibility of graphene depends on the applied magnetic field, in the limit of strong magnetic field [32]. In a recent work, moreover, the role of a constant, out-of-plane magnetic field in the nonlinear response of graphene was thoroughly investigated, revealing the possibility to use the magnetic field strength to control the frequency conversion, up to the visible range [33]. None of these works, however, investigated the role SOC might have in shaping the nonlinear optical response of graphene and, more generally, 2D materials.

In this work, we investigate the effects of both intrinsic and Rashba SOC on the nonlinear signal generated by an ultrashort electromagnetic pulse impinging upon a flake of bent graphene. To do so, we extend the formalism recently developed by one of the authors in Ref. [33] to explicitly account for the presence of a nonzero SOC coupling and explicitly accommodate spin dynamics in the model. For the

*marco.ornigotti@tuni.fi

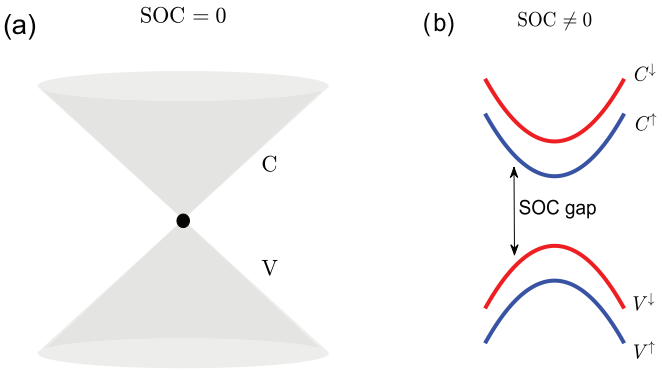

FIG. 1. Band structure of graphene in the vicinity of one Dirac valley (for example, K) for both (a) the case of no SOC, where the usual gapless, linear dispersion relation appears, and (b) the case with SOC. Depending on the kind of SOC considered, a gap can be opened at the Dirac point (intrinsic SOC), and the spin degeneracy of both valence and conduction bands can be lifted (Rashba SOC).

case of intrinsic SOC, in particular, we exploit the fact that the spin degeneracy of the electronic bands is lifted, and we introduce a spin-field interaction Hamiltonian and compare its action with the standard sublattice (i.e., minimal coupling) interaction Hamiltonian. Our results show that by addressing directly the spin degree of freedom of Dirac electrons in graphene it is possible, by controlling the level of intrinsic SOC, to significantly broaden the spectrum of the nonlinear signal, allowing efficient conversion of light from the terahertz (THz) to the UV region.

This work is organized as follows: in Sec. II we present the basic model used in this work, namely, the Hamiltonian for a 2D material (graphene, in this specific case) in the presence of SOC. Section III is then dedicated to the case of bent graphene and to deriving its eigenstates and eigenvalues for the cases of both intrinsic and Rashba SOC. In Sec. IV, we briefly discuss how to introduce the spin-field interaction in the graphene Hamiltonian and discuss explicitly the cases of linear and circular polarization. Section V is then dedicated to the discussion of the nonlinear signal in the presence of SOC. Finally, conclusions are drawn in Sec. VI.

II. GRAPHENE HAMILTONIAN WITH SOC

Electron dynamics in graphene are typically described using a four-component spinor, $\Phi(\mathbf{r},t)=(\phi_K^A,\phi_K^B,\phi_{K'}^A,\phi_{K'}^B)^T$, where $\{A,B\}$ refer to the sublattice site (associated with the so-called pseudospin degree of freedom), referring to the two carbon atoms per unit cell, and the indices $\{K,K'\}$ indicate the two nonequivalent valleys in k space [8]. If SOC is present, the spin degeneracy of the two Dirac bands in each valley is lifted, leading to a spin-resolved four-band system in each valley (see Fig. 1). In this case, electron dynamics are completely described by means of an eight-component spinor $\Psi(\mathbf{r},t)\equiv(\Phi_\uparrow(\mathbf{r},t),\Phi_\downarrow(\mathbf{r},t))^T$, where $\{\uparrow,\downarrow\}$ is the spin index. To write the Hamiltonian for graphene in the presence of SOC, notice that $\Psi(\mathbf{r},t)$ depends on three independent degrees of freedom, namely, pseudospin (sublattice), spin, and valley, each spanning one of three different two-dimensional subspaces, i.e., $\Psi(\mathbf{r},t)\in\mathcal{H}\equiv\mathcal{H}_{\text{valley}}\otimes\mathcal{H}_{AB}\otimes\mathcal{H}_{\text{spin}}$, where each individual subspace $\mathcal{H}_\mu$ is spanned by its own set of Pauli matrices $\sigma_{x,y,z}^\mu$ and $\dim\{\mathcal{H}\}=8$. Since SOC does not mix the valley degree of freedom, we can factor out the valley degree of freedom and reorganize the elements of $\Psi(\mathbf{r},t)$ by introducing the spin-resolved valley spinor $\phi^\xi=(\phi_{\uparrow,A}^\xi,\phi_{\uparrow,B}^\xi,\phi_{\downarrow,A}^\xi,\phi_{\downarrow,B}^\xi)^T$, with $\xi=\{1,-1\}\equiv\{K,K'\}$ being the valley index, so that $\Psi(\mathbf{r},t)=(\phi^K,\phi^{K'})^T$. By doing so, we can then write the single-valley Hamiltonian in the presence of SOC as

$$\hat{H}^\xi=\hat{H}_0^\xi+\hat{H}_I^\xi+\hat{H}_R^\xi, \tag{1}$$

where

$$\hat{H}_0^\xi=v_f(\xi\,p_x\,\mathbb{I}_s\otimes\sigma_x+p_y\,\mathbb{I}_s\otimes\sigma_y) \tag{2}$$

is the free Hamiltonian, $\mathbb{I}_s$ is the identity matrix in spin subspace, $\sigma_{x,y}$ are the Pauli matrices spanning the two-dimensional sublattice space $\mathcal{H}_{AB}$,

$$\hat{H}_I^\xi=\xi\,\Delta_I\,s_z\otimes\sigma_z \tag{3}$$

(with $s_{x,y}$ being the Pauli matrices spanning the two-dimensional spin space $\mathcal{H}_{\text{spin}}$) describes intrinsic SOC, which accounts for the case where the electron spin is oriented perpendicular to the graphene plane [8], and

$$\hat{H}_R^\xi=\Delta_R(\xi\,s_y\otimes\sigma_x-s_x\otimes\sigma_y) \tag{4}$$

is the Rashba Hamiltonian, describing the case in which the electron spin is oriented in the plane of graphene and it is responsible for the spin-momentum locking [8].

In graphene, the magnitude of both SOC terms is generally small, with the Rashba term being $\Delta_R\simeq 10\,\mu\text{eV}$ per V/nm [34], when an electric field is applied, and the intrinsic SOC term $\Delta_I\simeq 24\,\mu\text{eV}$ [35]. These effects, however, can be artificially enhanced by suitable adatom deposition, such as indium and thallium [23], or by putting the graphene sheet in contact with tellurite-based nanoparticles [24]. This results in an increase of the SOC of graphene of many orders of magnitude.

It is worth noticing that although in the remainder of this paper we will refer only to artificially enriched graphene, the model presented in this work can be easily adapted to any 2D material in the presence of SOC, such as transition-metal dichalcogenides (TMDs).

III. BENT GRAPHENE IN THE PRESENCE OF SOC

The discussion above is valid for an unstrained single layer of graphene. When strain, or bending, is taken into account, an artificial gauge field (AGF) emerges whose explicit expression depends on the nature of the strain or bending applied to the monolayer [36]. In the absence of out-of-plane modulations, such an induced AGF can be generally written as

$$\mathbf{A}^{(s)}=\pm C(u_{xx}-u_{yy})\hat{\mathbf{x}}\mp 2Cu_{xy}\hat{\mathbf{y}}, \tag{5}$$

where C is a suitable constant and $u_{\mu\nu}=\partial_\mu u_\nu-\partial_\nu u_\mu$ is the strain tensor [37]. Assuming a strain profile like the one described in Ref. [33] and pictorially represented in Fig. 2, we obtain an AGF $\mathbf{A}^{(s)}=-B\,y\,\mathbf{x}$, corresponding to a uniform magnetic field oriented perpendicular to the graphene plane, i.e., $\mathbf{B}=B\,\hat{\mathbf{z}}$. The interaction of electrons in graphene with the AGF defined above can be introduced through minimal

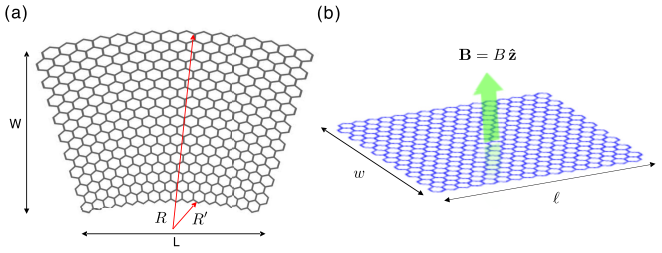

FIG. 2. (a) Pictorial representation of a rectangular flake of graphene, deformed into an arc. (Adapted from Ref. [33].) The radii of the upper and lower edges are, respectively, R and R'. (b) Flattened equivalent geometry of the bent graphene flake in (a). The curvature induced by the bending is replaced with an artificial gauge field $\mathbf{A}_s$, which gives rise to a uniform pseudomagnetic field $\mathbf{B} = B\,\hat{\mathbf{z}}$ parallel to the z direction. The width w and length ℓ of the flattened flake can be calculated from the bent structure and might be extended to infinity for making calculations easier, as this operation does not change the essential role the pseudomagnetic field has in light-matter interaction.

coupling, namely, by replacing the kinetic momentum $\mathbf{p}$ of the electron with the canonical momentum, i.e., $\mathbf{p} \mapsto \mathbf{p} + e\mathbf{A}^{(s)}$, in Eq. (2). This is equivalent to introducing a magnetic interaction Hamiltonian

$$\hat{H}_B^{\xi} = e\,v_F\,\xi\,A_x^{(s)}\,\mathbb{I}_s \otimes \sigma_x = -v_F\,e\,B\,y\,\xi\,\mathbb{I}_s \otimes \sigma_x \tag{6}$$

into Eq. (2). Since we are also considering the electron spin as a degree of freedom, simply adding the interaction term above to Eq. (2) is not enough, as we have to add an extra term to account for the interaction of the electron spin with the synthetic magnetic field, i.e., a Zeeman term of the following form [38]:

$$\hat{H}_Z = \Delta_Z\,s_z \otimes \mathbb{I}_{AB}, \tag{7}$$

where $\mathbb{I}_{AB}$ is the identity matrix in sublattice space and $\Delta_Z = g_s\mu_B B/2$ (with g_s being the gyromagnetic factor and μ_B being the Bohr magneton).

The total single-valley Hamiltonian for SOC in the presence of an AGF is then given by $\hat{H}_{\rm tot}^{\xi} = \hat{H}^{\xi} + \hat{H}_B^{\xi} + \hat{H}_Z^{\xi}$, and we can use it in the Dirac equation for electrons in the presence of SOC and under the action of an AGF as follows:

$$i\hbar\frac{\partial}{\partial t}|\psi(\mathbf{r},t)\rangle = \sum_{\xi=\pm1}\hat{H}_{\rm tot}^{\xi}\,|\psi^{\xi}(\mathbf{r},t)\rangle. \tag{8}$$

To solve the above equation, we write $|\psi(\mathbf{r},t)\rangle$ as a linear combination of the instantaneous eigenstates of $\hat{H}_{\rm tot}^{\xi}$ with time-dependent expansion coefficients [39]. To do so, although $\hat{H}_{\rm tot}^{\xi}$ admits closed-form eigenstates in the form of parabolic cylinder functions for the general case of both intrinsic and Rashba SOC present in the system [28], in this work we discuss the two cases separately. This will provide a much easier framework and will allow us to gain better insight into the role each of these two mechanisms plays in the nonlinear optical response of graphene.

A. Instantaneous eigenstates of $\hat{H}_{\rm tot}^{\xi}$ for only intrinsic SOC

To start with, we neglect Rashba coupling and set $\Delta_R = 0$. As intrinsic SOC cannot lift the spin degeneracy of the bands near the Dirac point and only introduces a nonzero gap proportional to Δ_I, the two spin states $\{|\uparrow\rangle, |\downarrow\rangle\}$ can be treated independently, and the spin index $\beta = \pm1 \equiv \{\uparrow, \downarrow\}$ enters only as a parameter (and not as a quantum number) in the expression of the eigenstates and eigenvalues of $\hat{H}_{\rm tot}^{\xi}$. As a result, we can then write the single-valley–single-spin Hamiltonian as

$$\begin{aligned}\hat{H}_{\beta}^{\xi} &= v_f(\xi\,p_x\sigma_x + p_y\sigma_y - e\,B\,y\,\xi\,\sigma_x)\\ &\quad + \beta(\xi\,\Delta_I\,\sigma_z + \Delta_Z),\end{aligned} \tag{9}$$

and then $\hat{H}_{\rm tot}^{\xi} = \hat{H}_{\uparrow}^{\xi} \otimes \hat{H}_{\downarrow}^{\xi}$, and therefore, $|\psi^{\xi}(\mathbf{r},t)\rangle = |\psi_{\uparrow}^{\xi}(\mathbf{r},t)\rangle \otimes |\psi_{\downarrow}^{\xi}(\mathbf{r},t)\rangle$.

Written in the form above, it is easy to recognize Eq. (9) as a gapped Landau Hamiltonian whose eigenvalues and eigenstates can be written in terms of harmonic oscillator eigenstates in the y direction as [40]

$$\left|\psi_{n,\beta}^{\xi}(y,t;p_x)\right\rangle = \mathrm{N}_{n,\beta}^{\xi}e^{i(\xi\frac{p_x}{\hbar}x - \frac{E_{n,\beta}^{\xi}}{\hbar}t)}\left|\Phi_{n,\beta}^{\xi}(\eta)\right\rangle, \tag{10}$$

with

$$\left|\Phi_{n,\beta}^{\xi,\alpha}(\eta)\right\rangle = \hat{O}(\xi)\begin{pmatrix}\nu_{n,\beta}^{\alpha}\,\phi_{n-1}(\eta)\\ \phi_n(\eta)\end{pmatrix}, \tag{11}$$

where $\hat{O}(\xi) = \mathbb{I}$ for $\xi = 1$ (K valley) and $\hat{O}(\xi) = -\sigma_z\sigma_x$ for $\xi = -1$ (K' valley). Here, $\phi_n(\eta)$ are normalized one-dimensional harmonic oscillator eigenstates [41] [with $\phi_{-1}(\eta) = 0$], $\eta = (-y + 2\ell_B^2\xi p_x)/\ell_B$ (with $\ell_B = \sqrt{\hbar/eB}$ being the magnetic length), $\mathrm{N}_{n,\beta}^{\xi}$ is a normalization constant,

$$\nu_{n,\beta}^{\alpha} = \frac{E_{n,\beta}^{\alpha} - E_0^{\alpha}}{\hbar\omega_c\sqrt{n}}, \tag{12}$$

and $E_{n,\beta}^{\alpha} = \alpha\hbar\omega_c\sqrt{n + (\Delta_I/\hbar\omega_c)^2} + \beta\Delta_z$ are the eigenvalues of Eq. (9) (with $\omega_c = v_F\sqrt{2}/\ell_B$ being the cyclotron frequency). $n \in \mathbb{N}_0$ indicates the Landau levels in the conduction ($\alpha = 1$) and valence ($\alpha = -1$) bands. Notice, moreover, that since the total Hamiltonian factors in spin space, there cannot be a common $n = 0$ Landau level, as in the case of no intrinsic SOC [33], but rather two separate levels, with spin-dependent eigenvalues $E_{0,\beta} = -\beta(\Delta_I - \Delta_Z)$ and spin-polarized eigenstates

$$\left|\Phi_{0,\beta}^{\xi}\right\rangle = \left(\frac{1}{2\pi}\right)^{1/4}\begin{pmatrix}0\\ \phi_0(\eta)\end{pmatrix}. \tag{13}$$

The corresponding band structure in the vicinity of the Dirac point for the first few Landau levels is shown schematically in Fig. 3.

B. Instantaneous eigenstates of $\hat{H}_{\rm tot}^{\xi}$ for only Rashba SOC

We now turn our attention to the case where only Rashba SOC is present; that is, we set $\Delta_I = 0 = \Delta_Z$ in the total Hamiltonian. Since the Rashba coupling term Δ_R introduces a coupling between the spin states, we cannot factor $\hat{H}_{\rm tot}^{\xi}$ in block-diagonal form anymore. We then need to deal with the full four-dimensional Hamiltonian $\hat{H}_{\rm tot}^{\xi} = \hat{H}^{\xi} + \hat{H}_R^{\xi}$. Its eigenstates and eigenvalues, however, can still be computed analytically, and they can still be expressed in terms of

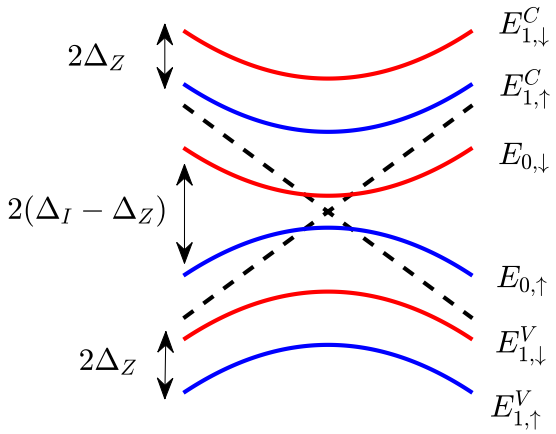

FIG. 3. First few Landau energy levels in the vicinity of the Dirac point in the presence of intrinsic SOC. As can be seen, the main effect of the intrinsic SOC is to open a gap between valence and conduction bands (lifting the band degeneracy at the Dirac point). The lifting of the spin degeneracy of each level is due to the Zeeman coupling. The dashed lines, depicting the band structure of unperturbed, pristine graphene, have been added to help the visualization of the band structure.

harmonic oscillator states [28] as follows:

$$\left|\psi^{\xi,\alpha}_{n,\beta}(y,t;p_x)\right\rangle = \mathrm{N}^{\alpha}_{n,\beta} e^{i(\xi\frac{p_x}{\hbar}x - \frac{E^{\alpha}_{n,\beta}}{\hbar}t)}\left|\Sigma^{\alpha}_{n,\beta}(\eta)\right\rangle, \tag{14}$$

where now $n \in \mathbb{Z}$ and

$$\left|\Sigma^{\alpha}_{n,\beta}(\eta)\right\rangle = \begin{pmatrix} i\,n\,\Delta_R\,a_{n-1}\phi_{n-1}(\eta) \\ i\,\Delta_R\,E^{\alpha}_{n,\beta}\,a_n\phi_n(\eta) \\ \left[\left(E^{\alpha}_{n,\beta}\right)^2 - n\right]a_n\phi_n(\eta) \\ \left[\frac{\left(E^{\alpha}_{n,\beta}\right)^2 - n}{E^{\alpha}_{n,\beta}}\right]a_{n+1}\phi_{n+1}(\eta) \end{pmatrix}, \tag{15}$$

where $a_n = \sqrt{n!}$ and $E^{\alpha}_{n,\beta}$ are the eigenvalues of $\hat{H}^{\xi}_{\mathrm{tot}}$, whose explicit expression is, in general, a complicated function of Δ_R and $\hbar\omega_c$ (see Ref. [28] for details). For the particular case $\varepsilon = \Delta_R/\hbar\omega_c \ll 1$, i.e., small Rashba coupling, however, we can find the following approximate analytical expression for the eigenvalues:

$$E^{\alpha}_{n,+} = \alpha\hbar\omega_c\left(1 + \frac{\varepsilon^2}{2}\right)\sqrt{n+1} + O(\varepsilon^4), \tag{16a}$$

$$E^{\alpha}_{n,-} = \alpha\hbar\omega_c\left(1 - \frac{\varepsilon^2}{2}\right)\sqrt{n} + O(\varepsilon^4). \tag{16b}$$

Notice that in this limit $\hat{H}^{\xi}_{\mathrm{tot}}$ admits two zero-energy states, one corresponding to $n = 0$ ($|\Sigma^{\xi,\alpha}_{0,-}\rangle$) and the other one corresponding to $n = -1$ ($|\Sigma^{\xi,\alpha}_{-1,+}\rangle$).

Notice, moreover, that for $\Delta_R = 0$, i.e., $\varepsilon = 0$ in Eq. (16), the condition $E^{\alpha}_{m-1,+} = E^{\alpha}_{m,-}$ holds, which implies a degeneracy of Landau levels. This degeneracy is then lifted for $\Delta_R > 0$, and in this case (and only this case) it makes sense to label the eigenstates with the index $\beta = \pm$, which, however, should not be associated with a genuine spin index since for the case of Rashba coupling, the bands are still degenerate in spin.

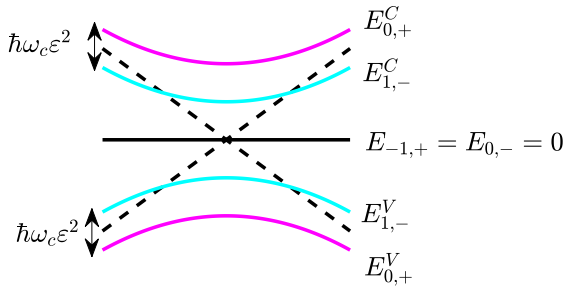

FIG. 4. Landau energy levels in the vicinity of the Dirac point for the case of nonzero Rashba coupling and for $n = \{0, 1\}$. Contrary to the case of intrinsic SOC, in this case we observe the presence of a doubly degenerate zero state. The dashed lines, depicting the band structure of unperturbed, pristine graphene, have been added to help with the visualization of the band structure.

The band structure in the vicinity of the Dirac point for the case of nonzero (but small) Rashba coupling, including the two zero-energy states and the states corresponding to $n = \{0, 1\}$ in both the valence and conduction bands, is reported in Fig. 4.

IV. INTERACTION WITH THE ELECTROMAGNETIC FIELD

We now consider the interaction of a flake of bent graphene in the presence of SOC with an external electromagnetic field, and we then calculate its nonlinear response. To account for such an interaction, we employ minimal coupling and simply make the electromagnetic vector potential $\mathbf{A}(t)$ appear via the minimal substitution $\mathbf{p} \mapsto [\mathbf{p} + e\mathbf{A}^{(s)} + e\mathbf{A}(t)]$, so that the effects of both an actual (electromagnetic pulse) and artificial (bending) gauge field are described within the same formalism. Throughout this whole section, we assume the electromagnetic vector potential is written as $\mathbf{A}(t) = \mathcal{A}(t)e^{-i\omega_L t}\hat{\mathbf{f}} + \mathrm{c.c.}$, where $\hat{\mathbf{f}}$ is a suitable polarization vector, ω_L is the pulse carrier frequency, and the pulse shape is assumed to be Gaussian, i.e., $\mathcal{A}(t) = E_L\tau\,\exp[-(t-t_0)^2/\tau^2]$, with E_L being the pulse amplitude and τ being its duration. We, moreover, assume for simplicity that the electromagnetic field impinges normally on the bent graphene sheet. This assumption is justified by the fact that our model Hamiltonian for graphene automatically takes into account a recentering of k space around the position of the Dirac points.

Accounting for all the aforementioned assumptions, in this section we will therefore consider the following form of the single-valley Dirac equation:

$$i\hbar\frac{\partial}{\partial t}|\Psi^{\xi}(x,y,t)\rangle = \left[\hat{H}^{\xi}_{\mathrm{tot}} + \hat{H}_{\mathrm{int}}(t)\right]|\Psi^{\xi}(x,y,t)\rangle, \tag{17}$$

where the interaction term $\hat{H}_{\mathrm{int}}(t)$ will assume different explicit forms, depending on the kind of interaction we are considering, as discussed below.

In general, however, the interaction term $\hat{H}_{\mathrm{int}}(t)$ can be gauged by means of the phase transformation

$$|\Psi^{\xi}(x,y,t)\rangle = \int dp_x\, e^{i\frac{p_x}{\hbar}x}e^{-i\hat{G}(t)}|\psi^{\xi}(y,t;p_x)\rangle, \tag{18}$$

where $\hat{G}(t) = \hbar^{-1}\int_0^t ds\,\hat{H}_{\rm int}(s)$. Following the reasoning from Ref. [33], we can calculate the instantaneous eigenstates of the equation above, which we define as $|\Theta^{\xi,\alpha}_{n,\beta}(t)\rangle$, for which we have $|\Theta^{\xi,\alpha}_{n,\beta}(t)\rangle = |\Phi^{\xi,\alpha}_{n,\beta}(t)\rangle$ for the case of intrinsic SOC and $|\Theta^{\xi,\alpha}_{n,\beta}(t)\rangle = |\Sigma^{\xi,\alpha}_{n,\beta}(t)\rangle$ for the case of Rashba coupling.

To solve Eq. (17), we then employ the ansatz

$$|\psi^{\xi}(y,t;p_x)\rangle = e^{-i\hat{G}(t)}\sum_{n,\alpha,\beta} c^{\xi,\alpha}_{n,\beta}(t)\big|\Theta^{\xi,\alpha}_{n,\beta}(y,t;p_x)\big\rangle, \tag{19}$$

which amounts to considering the general electron dynamics for SOC bent graphene interacting with an external field as a weighted superposition of instantaneous Landau eigenstates. Substituting this ansatz into Eq. (17) leads to solving a differential equation system for the expansion coefficients $c^{\alpha}_{n,\beta}(t)$:

$$\dot{c}^{\xi,\alpha'}_{m,\beta'}(t) = i\sum_{n}\sum_{\alpha,\beta}\big\langle\Theta^{\xi,\alpha'}_{m,\beta'}\big|\hat{H}_{\rm int}(t)\big|\Theta^{\xi,\alpha}_{n,\beta}\big\rangle c^{\xi,\alpha}_{n,\beta}(t), \tag{20}$$

where $\alpha,\beta = \{-1,1\}$. Notice that the states $|\Theta^{\xi,\alpha}_{n,\beta}\rangle$ are orthogonal with respect to the index n and the number of eigenstates involved in the sum above is essentially regulated by the initial conditions.

We then consider two different regimes of light-matter interaction: first, we consider the usual sublattice coupling and assume that the impinging electromagnetic field is linearly polarized along the x direction (namely, the one indicated by ℓ in Fig. 2); that is, we choose $\hat{\mathbf{f}} = \hat{\mathbf{x}}$. The minimal coupling Hamiltonian in this case reads

$$\hat{H}_{\rm int}(t) = e\,v_F\,\mathbb{I}_s\otimes\xi\,A_x(t)\,\sigma_x. \tag{21}$$

Second, we introduce a spin-field interaction term which couples the photon and electron spin directly, thus granting us access to spin dynamics. To do so, we consider the case of a circularly polarized pulse, for which we choose $\hat{\mathbf{f}} = \hat{\mathbf{h}}_\lambda$, where $\hat{\mathbf{h}}_\lambda = (\hat{\mathbf{x}} + i\lambda\hat{\mathbf{y}})/\sqrt{2}$ is the helicity basis [42] and $\lambda = \pm 1$ is the photon spin angular momentum (SAM), corresponding to left-handed ($\lambda = +1$) or right-handed ($\lambda = -1$) circular polarization. In this case, since the impinging pulse is carrying SAM, we can introduce an extra interaction Hamiltonian that describes the SAM-electron spin interaction, rather than the usual sublattice interaction described by Eq. (21), of the form

$$\hat{H}^{\rm SF}_{\rm int}(t) = e\,v_F\,A_\mu(t)\,s_\mu\otimes\mathbb{I}_{AB}, \tag{22}$$

where the superscript SF stands for *spin field* to emphasize the nature of the interaction and distinguish the above interaction Hamiltonian from Eq. (21).

Notice that $\hat{H}^{\rm SF}_{\rm int}(t)$ makes sense as interaction Hamiltonian only when the electron spin can be addressed as an independent degree of freedom, namely, only in the intrinsic SOC case, with a nonzero Zeeman effect. In all other cases, where the spin degeneracy is not lifted, the interaction Hamiltonian cannot be written in this form, as one would not be able to define Pauli matrices for the spin states since spin is not an available degree of freedom.

Dirac current and nonlinear signal

The nonlinear response of graphene can be estimated by first calculating the electric current generated by the interaction of the electromagnetic field with the graphene layer, namely,

$$J^{\xi}_{\mu}(t) = \int dx\,dy\,\langle\Psi^{\xi}|\hat{\mathcal{J}}_\mu|\Psi^{\xi}\rangle, \tag{23}$$

where $\hat{\mathcal{J}}_\mu$ is a suitable current operator whose definition depends on the kind of interaction described above, namely, $\hat{\mathcal{J}}_\mu = \mathbb{I}_s\otimes\sigma_\mu$ for the interaction described by Eq. (21) and $\hat{\mathcal{J}}_\mu = s_\mu\otimes\mathbb{I}_{AB}$ for the spin-field interaction described by Eq. (22). From the Dirac current, we can then calculate the spectrum of the emitted radiation, the so-called nonlinear signal, as a function of frequency as

$$I(\omega)\propto|\omega\,\tilde{\mathbf{J}}(\omega)|^2, \tag{24}$$

where $\tilde{\mathbf{J}}(\omega)$ is the Fourier transform of the Dirac current $\mathbf{J}(t)$.

V. NONLINEAR SIGNAL

We now have all the tools needed to investigate the nonlinear response of bent graphene in the presence of artificially enhanced SOC, considering the effects of both the sublattice and spin-field interactions. We assume a pseudomagnetic field of magnitude $B = 2$ T and an impinging electromagnetic pulse with amplitude $E_L = 10^7$ V/m and a duration of $\tau = 50$ fs, with a carrier frequency of $\omega_L = 78$ THz, fully resonant with the transition from between the lowest and the zeroth state in the case of no SOC and nearly resonant between the lowest and second-lowest states in the case when SOC is present. As initial conditions, we assume, for the cases of both intrinsic and Rashba SOC, $\mathbf{c}^T(0) = (1\,0\,0\,1\,0\,0)^T/\sqrt{2}$. For the case of intrinsic SOC, this initial condition corresponds to assuming equal populations of the lowest spin-up and spin-down states, i.e., $\mathbf{c}^T(0) = (c^V_{1,\uparrow}(0)\,c_{0,\uparrow}(0)\,c^C_{1,\uparrow}(0)\,c^V_{1,\downarrow}(0)\,c_{0,\downarrow}(0),\,c^C_{1,\downarrow}(0))^T$. For the case of Rashba coupling, on the other hand, since spin is not a viable quantum number anymore, the initial condition above just reduces to assuming equal populations in the $+$ and $-$ states of the valence band since $\mathbf{c}^T(0) = (c^V_{1,-}(0)\,c_{0,-}(0)\,c^C_{1,-}(0)\,c^V_{0,+}(0)\,c_{-1,+}(0)\,c^C_{0,+}(0))^T$.

A. Linear polarization

We start by first discussing the case of sublattice coupling with an x-polarized impinging field. To this aim, we mainly consider the effect of intrinsic (Δ_I) SOC because, as we will show, the influence of Rashba (Δ_R) SOC is not very significant. To corroborate this statement, we first performed simulations using typical values of both intrinsic and Rashba SOC for the case of artificially enhanced graphene, and we chose $\Delta_I = 5$ meV and $\Delta_R = 15$ meV. The result of these simulations is reported in Fig. 5. As can be seen from Fig. 5(a), the presence of SOC of any kind does not drastically change the nonlinear response of bent graphene, but rather introduces small changes, mainly in the spectral region around the fundamental frequency and in the high-harmonics region.

Let us first discuss the impact of the Rashba coupling (pink line in Fig. 5). We see from Fig. 5(b) that the main spectral region where Rashba SOC affects the nonlinear signal is the low-frequency region, around the fundamental frequency $\omega_L = \omega_1$. In this region, in fact, the nonlinear spectrum

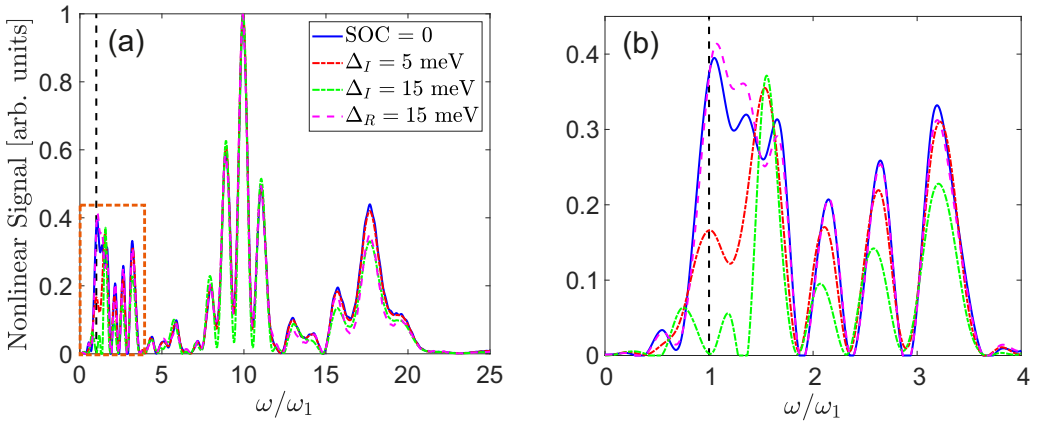

FIG. 5. (a) Spectrum of radiation emitted by artificially enhanced bent graphene for the case of impinging x polarization and (b) a zoom of the low-frequency part of the spectrum, i.e., $0 \leqslant \omega \leqslant 4\omega_1$. The black dashed line indicates the position of the fundamental frequency (i.e., $\omega = \omega_L = \omega_1$). The solid blue line corresponds to the case of no SOC and serves as a reference for the discussion. The red and green dashed lines represent, respectively, low and high intrinsic SOC achievable with usual enhancement processes, while the pink dashed line represents the same situation, but for the Rashba coupling. For these plots, the following parameters are used: $\tau = 50$ fs, $\omega_L = 78$ THz, $B = 2$ T, and $E_L = 10^7$ V/m.

near the fundamental is slightly deformed. Overall, however, Fig. 5 clearly shows how even a big chosen value of $\Delta_R = 15$ does not introduce significant changes in the nonlinear spectrum. This observation then allows us to conclude that Rashba SOC does not really contribute significantly to the nonlinear signal and cannot therefore be used as an active control parameter to shape and engineer the nonlinear response of bent graphene.

On the other hand, we clearly see from Fig. 5(b) that the intrinsic SOC has a much higher impact on the nonlinear response of bent graphene. In fact, although we can see from Fig. 5(a) that a significant change in magnitude of the SOC from $\Delta_I = 5$ meV (dashed red line) to $\Delta_I = 15$ meV (dashed green line) does not have a great impact on the high-frequency side of the spectrum, where it introduces only a slight redistribution of energy [see, for example, the Δ_I-dependent peak modulation around the 18th harmonic in Fig. 5(a)], it has quite a significant impact on the low-frequency part of the nonlinear signal. A careful investigation of Fig. 5(b), in fact, reveals that although the usual harmonic-oscillator-like structure of low-order harmonics [33] is preserved also in the case of SOC, higher values of Δ_I tend to redistribute energy around the second harmonic in a more efficient way than lower (or absent) values of SOC. For $\Delta_I = 15$ meV, in particular, we see the emergence of a train of almost equally spaced noninteger harmonics, covering the range $[\omega_L, 4\,\omega_L]$.

This observation sparks the interesting question of whether this trend can be pushed forward and intrinsic SOC can be used to effectively control the shape of the nonlinear response, at least in some frequency region. If this were the case,

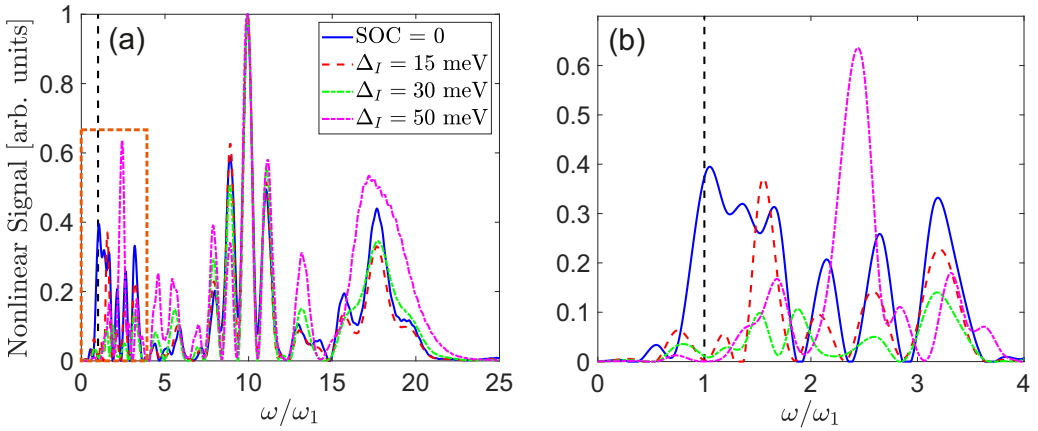

FIG. 6. (a) Spectrum of radiation emitted by artificially enhanced bent graphene for the case of impinging x polarization and (b) a zoom of the low-frequency part of the spectrum, i.e., $0 \leqslant \omega \leqslant 4\omega_1$. The black dashed line indicates the position of the fundamental frequency (i.e., $\omega = \omega_L = \omega_1$). The solid blue line corresponds to the case of no SOC and serves as a reference for the discussion. The dashed red line corresponds to $\Delta_I = 15$ meV and depicts the same situation as the green dashed line in Fig. 5. The dashed green and magenta lines correspond, respectively, to $\Delta_I = 30$ meV and $\Delta_I = 50$ meV. For these plots, the following parameters are used: $\tau = 50$ fs, $\omega_L = 78$ THz, $B = 2$ T, and $E_L = 10^7$ V/m.

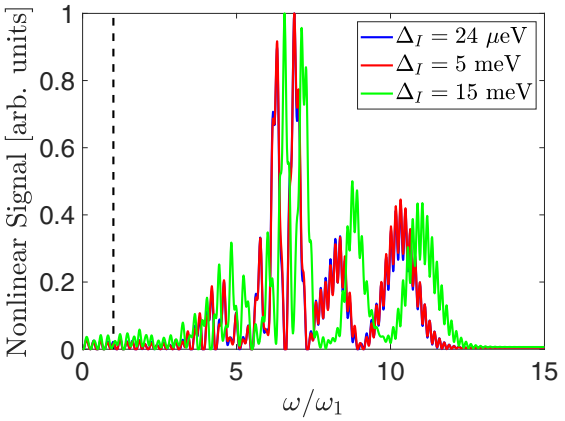

FIG. 7. Spectrum of emitted radiation in the case of a left-handed circularly polarized impinging pulse for the case of low intrinsic SOC values. The black dashed line indicates the position of the fundamental frequency (i.e., $\omega = \omega_L = \omega_1$). For this plot, the following parameters are used: $\tau = 50$ fs, $\omega_L = 160$ THz, $B = 2$ T, and $E_L = 10^7$ V/m.

artificially enhancing graphene could be a viable choice to tune its optical properties, even in "real time."

To this aim, in Fig. 6 we compare the nonlinear signal produced by artificially enhanced graphene with progressively increasing values of intrinsic SOC, i.e., $\Delta_I = 15$ meV (dashed red line in Fig. 6), $\Delta_I = 30$ meV (dashed green line in Fig. 6), and $\Delta_I = 50$ meV (dashed magenta line in Fig. 6). As can be seen, increasing the intrinsic SOC has different effects in different parts of the nonlinear spectrum. For high harmonics ($\omega \geqslant 15\omega_1$), increasing the amount of SOC in the system has the direct result of progressively broadening the harmonic peaks until, for $\Delta_I = 50$ meV, we obtain a single, broad peak with higher intensity than the initial harmonics (blue line in Fig. 6). For the range $5\omega_1 \leqslant 15\omega_1$, on the other hand, no significant changes seem to appear, as the basic structure of the nonlinear spectrum remains essentially the same, up to a small redistribution of energy between the harmonics. The situation for frequencies, i.e., $\omega \leqslant 5\omega_1$, however, is quite different, as can be seen from Fig. 6(b). While for small values of Δ_I the characteristic equally spaced spectrum is still visible, although slightly redshifted, for high values of Δ_I, the situation changes drastically as the harmonic-oscillator-like peaks, typical of the nonlinear response in this region [33], disappear and a single, intense peak appears at approximately the noninteger frequency $\omega = 5\omega/2$. Moreover, comparing the blue curve (no SOC) with all the others reveals how the presence of SOC makes the peak at the fundamental frequency $\omega = \omega_1$ disappear, meaning that SOC encourages a total redistribution of energy from the pump pulse to the different harmonics created in the material. This is an indication of how SOC can be used to tune the nonlinear response of artificially enhanced graphene to generate devices for efficient conversion of light to specific frequencies that do not need to be integer multiples of some fundamental frequency.

To conclude this section, we would like to point out that although this situation is highly unlikely to be observed in graphene, where even with artificial enrichment the SOC values achievable still remain in the meV regime, our results could be useful to describe the effect of SOC on the nonlinear signal of 2D materials in general, whose electronic properties can be described by a graphene-like Hamiltonian. TMDs, in particular, are a good example of that since SOC is already quite large in such materials and it could be enhanced even further with techniques similar to those utilized for graphene.

B. Circular polarization

We now turn our attention to the spin-field interaction Hamiltonian and investigate what kind of nonlinear signal such an interaction reveals. Here, as we did in the previous section, we concentrate on only intrinsic SOC and discuss the cases for both small and large values of Δ_I, whose results are depicted in Figs. 7 and 8, respectively. In both figures, the laser parameters are the same as those used for the case of linear polarization, except for the carrier frequency, which in Fig. 8 changes with increasing SOC to match the different values of SOC used for the simulations, so that the impinging electromagnetic pulse will always be resonant with an actual transition between a level in the valence band and one in the conduction band and no detuning will be present.

For small values of Δ_I, as can be seen from Fig. 7, the situation is similar to the case of linear polarization, and no

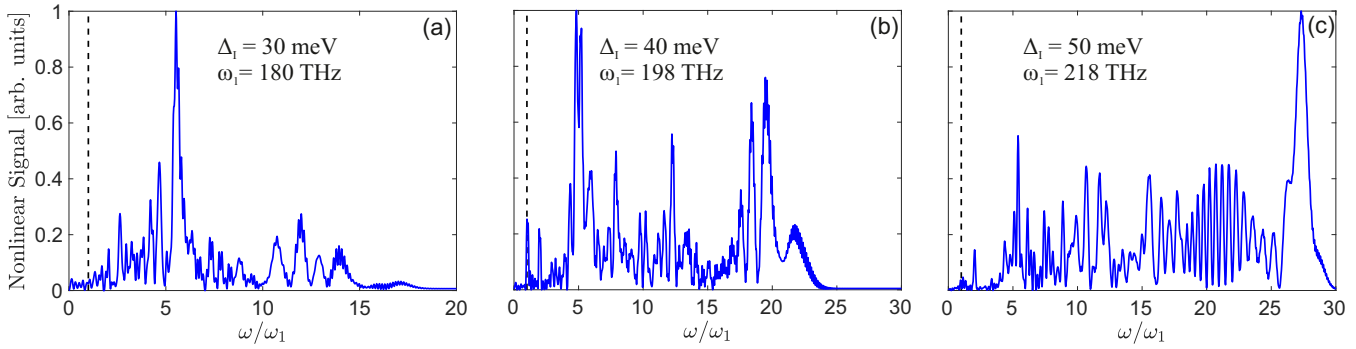

FIG. 8. Spectrum of emitted radiation in the case of a left-handed circularly polarized impinging pulse for the case of high SOC values. The laser frequency ω_L has been adjusted to the various levels of intrinsic SOC to ensure that the impinging pulse has no detuning. Notice how the spectrum broadens with increasing values of Δ_I, reaching, in (c), almost the 30th harmonic. The black dashed line indicates the position of the fundamental frequency (i.e., $\omega = \omega_L = \omega_1$). For these plots, the following parameters are used: $\tau = 50$ fs, $B = 2$ T, and $E_L = 10^7$ V/m.

appreciable changes can be observed. However, for values of $\Delta_I \geqslant 15$ meV (see the green line in Fig. 7), we start observing a significant blueshift of the nonlinear response. Notice, moreover, that the blueshift is not constant over the whole spectrum, and it is chirped in such a way that lower frequencies experience a smaller shift than the higher ones. This blueshift can be interpreted, with the help of Fig. 3, as the progressive increase of the gap between the (still equally spaced) Landau levels in valence and conduction bands, which become bigger as Δ_I increases.

If we increase Δ_I even further, as shown in Fig. 8, we witness a progressive broadening of the harmonic spectrum and the possibility, at very high SOC values [see Fig. 8(c)], of efficiently generating high-order harmonics. In particular, in the case shown in Fig. 8(c), we can excite the 28th harmonic of the fundamental frequency $\omega_L = 217$ THz, corresponding to a wavelength of about $\lambda_{28} = 310$ nm, well within the UV region of the electromagnetic spectrum.

VI. CONCLUSIONS

In this work, we theoretically investigated the effect of spin-orbit coupling on the nonlinear response of a sheet of graphene under the action of an artificial magnetic field for the cases of both Rashba and intrinsic SOC. The latter, in particular, allows for direct spin-field coupling via the Hamiltonian in Eq. (22), which shows interesting features.

Our results show that although for realistic values of both intrinsic and Rashba SOC in graphene no significant changes are induced in the nonlinear signal by SOC, controlling the amount of intrinsic SOC in 2D materials in the presence of an artificial magnetic field can result in a broadening of the spectrum of harmonics and can even allow efficient conversion of light from the THz to UV regions of the electromagnetic spectrum. This might lead to novel ways of generating spatially varying frequency-generation devices based on 2D materials, which could be achieved, for example, by inhomogeneously depositing SOC-active compounds over the surface of the 2D material, thus creating a *de facto* gradient of intrinsic SOC through the material surface.

ACKNOWLEDGMENT

The authors acknowledge the financial support from the Academy of Finland Flagship Programme, Photonics Research and Innovation (PREIN), Decision No. 320165.

[1] K. S. Novoselov, A. K. Geim, S. V. Morozov, D. Jiang, Y. Zhang, S. V. Dubonos, I. V. Grigorieva, and A. A. Firsov, Electric field effect in atomically thin carbon films, Science **306**, 666 (2004).

[2] A. C. Ferrari *et al.*, Science and technology roadmap for graphene, related two-dimensional crystals, and hybrid systems, Nanoscale **7**, 4598 (2015).

[3] K. S. Novoselov, V. I. Fal'ko, L. Colombo, P. R. Gellert, M. G. Schwab, and K. Kim, A roadmap for graphene, Nature (London) **490**, 192 (2012).

[4] R. R. Nair, P. Blake, A. N. Grigorenko, K. S. Novoselov, T. J. Booth, T. Stauber, N. M. R. Peres, and A. K. Geim, Fine structure constant defines visual transparency of graphene, Science **320**, 1308 (2008).

[5] Z. Sun, T. Hasan, F. Torrisi, D. Popa, G. Privitera, F. Wang, F. Bonaccorso, D. M. Basko, and A. C. Ferrari, Graphene mode-locked ultrafast laser, ACS Nano **4**, 803 (2010).

[6] Z. Sun, A. Martinez, and F. Wang, Optical modulators with 2D layered materials, Nat. Photon. **10**, 227 (2016).

[7] X. Liu, Q. Guo, and J. Qiu, Emerging low-dimensional materials for nonlinear optics and ultrafast photonics, Adv. Mater. **29**, 1605886 (2017).

[8] M. I. Katsnelson, *Graphene: Carbon in Two Dimensions* (Cambridge University Press, Cambridge, 2012).

[9] C. L. Kane and E. J. Mele, Quantum Spin Hall Effect in Graphene, Phys. Rev. Lett. **95**, 226801 (2005).

[10] M. Z. Hasan and C. L. Kane, Colloquium: Topological insulators, Rev. Mod. Phys. **82**, 3045 (2010).

[11] L. Lu, J. Joannopoulos, and M. Soljačić, Topological photonics, Nat. Photon. **8**, 821 (2014).

[12] T. Ozawa, H. M. Price, A. Amo, N. Goldman, M. Hafezi, L. Lu, M. C. Rechtsman, D. Schuster, J. Simon, O. Zilberberg, and I. Carusotto, Topological photonics, Rev. Mod. Phys. **91**, 015006 (2019).

[13] S. D. Huber, Topological mechanics, Nat. Phys. **12**, 621 (2016).

[14] N. Goldman, J. C. Budich, and P. Zoller, Topological quantum matter with ultracold gases in optical lattices, Nat. Phys. **12**, 639 (2016).

[15] D. Huertas-Hernando, F. Guinea, and A. Brataas, Spin-orbit coupling in curved graphene, fullerenes, nanotubes, and nanotube caps, Phys. Rev. B **74**, 155426 (2006).

[16] H. Min, J. E. Hill, N. A. Sinitsyn, B. R. Sahu, L. Kleinman, and A. H. MacDonald, Intrinsic and Rashba spin-orbit interactions in graphene sheets, Phys. Rev. B **74**, 165310 (2006).

[17] Y. Yao, F. Ye, X.-L. Qi, S.-C. Zhang, and Z. Fang, Spin-orbit gap of graphene: First-principles calculations, Phys. Rev. B **75**, 041401(R) (2007).

[18] M. König, H. Buhmann, L. W. Molenkamp, T. Hughes, C.-X. Liu, X.-L. Qi, and S.-C. Zhang, The quantum spin Hall effect: Theory and experiment, J. Phys. Soc. Jpn. **77**, 031007 (2008).

[19] L. Du, I. Knez, G. Sullivan, and R.-R. Du, Robust Helical Edge Transport in Gated InAs/GaSb Bilayers, Phys. Rev. Lett. **114**, 096802 (2015).

[20] X. Qian, J. Liu, L. Fu, and J. Li, Quantum spin Hall effect in two-dimensional transition metal dichalcogenides, Science **346**, 1344 (2014).

[21] Yu. S. Dedkov, M. Fonin, U. Rüdiger, and C. Laubschat, Rashba Effect in the Graphene/Ni(111) System, Phys. Rev. Lett. **100**, 107602 (2008).

[22] A. Varykhalov, J. Sánchez-Barriga, A. M. Shikin, C. Biswas, E. Vescovo, A. Rybkin, D. Marchenko, and O. Rader, Electronic and Magnetic Properties of Quasifreestanding Graphene on Ni, Phys. Rev. Lett. **101**, 157601 (2008).

[23] C. Weeks, J. Hu, J. Alicea, M. Franz, and R. Wu, Engineering a Robust Quantum Spin Hall State in Graphene via Adatom Deposition, Phys. Rev. X **1**, 021001 (2011).

[24] K. Hatsuda, H. Mine, T. Nakamura, J. Li, R. Wu, S. Katsumoto, and J. Haruyama, Evidence for a quantum spin Hall phase in graphene decorated with Bi_2Te_3 nanoparticles, Sci. Adv. **4**, eaau6915 (2018).

[25] A. H. Castro Neto and F. Guinea, Impurity-Induced Spin-Orbit Coupling in Graphene, Phys. Rev. Lett. **103**, 026804 (2009).

[26] D. Huertas-Hernando, F. Guinea, and A. Brataas, Spin-Orbit-Mediated Spin Relaxation in Graphene, Phys. Rev. Lett. **103**, 146801 (2009).

[27] E. I. Rashba, Graphene with structure-induced spin-orbit coupling: Spin-polarized states, spin zero modes, and quantum Hall effect, Phys. Rev. B **79**, 161409(R) (2009).

[28] A. De Martino, A. Hütten, and R. Egger, Landau levels, edge states, and strained magnetic waveguides in graphene monolayers with enhanced spin-orbit interaction, Phys. Rev. B **84**, 155420 (2011).

[29] H. Rostami, R. Roldán, E. Cappelluti, R. Asgari, and F. Guinea, Theory of strain in single-layer transition metal dichalcogenides, Phys. Rev. B **92**, 195402 (2015).

[30] H. Rostami and R. Asgari, Electronic structure and layer-resolved transmission of bilayer graphene nanoribbon in the presence of vertical fields, Phys. Rev. B **88**, 035404 (2013).

[31] M. A. H. Vozmediano, M. I. Katsnelson, and F. Guinea, Gauge fields in graphene, Phys. Rep. **496**, 109 (2010).

[32] X. Yao and A. Belyanin, Nonlinear optics of graphene in a strong magnetic field, J. Phys.: Condens. Matter **25**, 054203 (2013).

[33] M. Ornigotti, L. Ornigotti, and F. Biancalana, Generation of half-integer harmonics and efficient THz-to-visible frequency conversion in strained graphene, APL Photon. **6**, 060801 (2021).

[34] M. Gmitra, S. Konschuh, C. Ertler, C. Ambrosch-Draxl, and J. Fabian, Band-structure topologies of graphene: Spin-orbit coupling effects from first principles, Phys. Rev. B **80**, 235431 (2009).

[35] S. Konschuh, M. Gmitra, and J. Fabian, Tight-binding theory of the spin-orbit coupling in graphene, Phys. Rev. B **82**, 245412 (2010).

[36] F. Guinea, M. I. Katsnelson, and A. K. Geim, Energy gaps and a zero-field quantum Hall effect in graphene by strain engineering, Nat. Phys. **6**, 30 (2010).

[37] F. Guinea, A. K. Geim, M. I. Katsnelson, and K. S. Novoselov, Generating quantizing pseudomagnetic fields by bending graphene ribbons, Phys. Rev. B **81**, 035408 (2010).

[38] L. Dell'Anna and A. De Martino, Wave-vector-dependent spin filtering and spin transport through magnetic barriers in graphene, Phys. Rev. B **80**, 155416 (2009).

[39] K. L. Ishikawa, Nonlinear optical response of graphene in time domain, Phys. Rev. B **82**, 201402(R) (2010).

[40] L. D. Landau and E. M. Lifshitz, *Quantum Mechanics: Nonrelativistic Theory* (Pergamon Press, Oxford, England, 1977).

[41] F. W. Byron and R. W. Fuller, *Mathematics of Classical and Quantum Physics* (Dover, Mineola, New York, 1992).

[42] L. Mandel and E. Wolf, *Optical Coherence and Quantum Optics* (Cambridge University Press, Cambridge, 1995).